# MAX-PLANCK-INSTITUT
## FÜR PLASMAPHYSIK

**INSTITUT NATIONAL DES SCIENCES APPLIQUÉES DE STRASBOURG**
Department of mechanical engineering
**UNIVERSITÉ DE STRASBOURG**
Faculty of Physics and Engineering

Master's Thesis submitted in fulfillment of the requirements for the degrees of
*Master of Engineering*
*Master of Science*

# Thermal and structural finite element analysis of ECRH reflector tile of Wendelstein 7-X

*Author:*
**Nicolas Olive-Leriche**
Mechanical engineering/Applied physics and physical engineering

*Academic supervisor:*
**MdC. MATHIEU SOLAR**
INSA Strasbourg
Institut Charles Sadron

*Professional tutor:*
**MIKHAIL KHOKHLOV**
Max Planck Institute for Plasma Physics

Greifswald, 2024

**Acknowledgement**

## Abstract

# Contents

# List of Figures

## Acronyms

# 1 | INTRODUCTION

NUCLEAR fusion has been the subject of many years of research and different experiments conducted at all scales. This craze is mainly due to the possibility of clean, renewable and safe nuclear power generation. This idea of generating electricity via the fusion of light atomic nuclei finds its roots in the early 1950s when physicists tried different ways of containing a plasma using different techniques, one of which is called magnetic confinement. To know why such devices are necessary, a look at the physics behind nuclear fusion could help. Fusing light atomic nuclei require them to come close enough for the strong nuclear force to overcome the electrostatic force pushing them apart. One way to approach one nucleus to the other close enough to surpass the so-called Coulomb barrier is to heat the atoms to high temperatures or accelerate those particles enough to attain such energies. At those energies, the fuel becomes a hot plasma and can no longer be contained in a classical confinement.

Plasma is the fourth state of matter, consisting of ionized gas where atoms lose electrons. This ionization results in a mixture of positively charged ions and free electrons, making plasma distinct from solids, liquids, and gases. Plasmas exhibit unique properties, including responsiveness to magnetic fields and the ability to conduct electricity. They are prevalent in phenomena like stars, lightning, and certain man-made technologies such as fluorescent lights and plasma TVs. The pursuit of effective confinement for fusion plasma introduces various challenges of a complex nature. Stability concerns arise from inherent plasma instabilities, contributing to disruptions and energy dissipation. The prudent management of heat generated by fusion reactions assumes paramount importance to mitigate potential damage to plasma facing components. The research for materials suitable for the plasma facing components with enhanced durability requires overcoming challenges associated with extreme conditions, including elevated temperatures, neutron bombardment, and erosion.

Magnetic confinement, a crucial aspect of fusion devices, necessitates intricate manipulation of magnetic fields to attain stability and sustain plasma confinement. Establishing an energy equilibrium, where input aligns with output, constitutes a foundational imperative for realizing ignition in fusion reactions. The control of turbulence and transport phenomena within the plasma is essential to preclude unwarranted particle and energy transport, optimizing overall performance. The delicate equilibrium governing plasma density and temperature, vital for sustained fusion reactions, necessitates meticulous control and stability. Addressing these intricacies assumes pivotal significance in advancing fusion research and realizing the potential of fusion energy as a scientifically viable and sustainable power source. Wendelstein 7-X (W7-X) is an experimental Stellarator fusion device located at the Max Planck Institute for Plasma Physics (IPP) in Greifswald, Germany. The purpose of W7-X is to investigate the feasibility of generating energy through nuclear fusion.

## 1.1 PROBLEM DEFINITION AND OBJECTIVES

W7-X enters its enhanced operation phase called OP2. This operation phase aims to improve confinement time and heating power. To achieve longer runs and attain steady state operation, many different plasma parameters such as the temperature, the density and the pressure need to be fully controlled and piloted precisely. To gain this control and understand more the complex plasma dynamics of the reactors, longer plasma discharges will take place and provide to the physicists the desired data. Because the plasma discharges are longer and the plasma heated at higher powers than in Operation Phase 1 OP1, the components surrounding the plasma, especially the plasma facing components (PFCs) will be exposed to higher heat flux for a longer period of time. This will lead to increased wear on the system components due to high heat fluxes and can lead to mechanical failure. To assess this risk of failure, the engineering analysis group of the Experimental Plasma Physics 5 department conducts many different numerical analysis campaigns to predict the behavior of the device under special load cases.

In order to set boundaries on the pulses of OP2 and validate the proper functioning of the various subsystems, the thermal analyses as well as the mechanical analyses of various in-vessel components both steady and unsteady is carried out by the engineers. After early calculations, it was shown that. It is necessary for the ECRH TZM-reflector tile to accommodate for high steady state heat flux. Steady state is assumed for the analysis since the plasma impulse is considered of long duration and the thermal equilibrium of the reflector tile attained. It is crucial to properly design and dimension the tile in order to allow the new operational parameters. Based on the modified TZM-reflector tile, thermal and structural finite element analyses of different load cases and boundary conditions BCs will be conducted to validate the new design. Following the results of these analyses, the engineers will be able to set operational boundaries if necessary or validate the design and proceed with the operation. The results will also allow to know the different maximum operational parameters such as maximum operation time. The reliability of the calculations will influence the decision made and thus needs to be estimated to avoid any significant error between the FE model and the real life behavior.

First, a literature research is carried out to understand the physics involved in those phenomenon such as the link between temperature and mechanical properties of materials or the physics of radiative heat transfer. The reading of documents assessing those issues also helps put into context this work and lie the basis upon which this Thesis is being lead. Because this is entirely simulation based, the proper functioning of the analyzed components will be proved by locating their performances within an operational space defined by the designers under various load cases and meshes. In addition to that, this work is separated into main tasks, the steady state as well as transient thermal and mechanical FEA of the ECRH TZM-reflector tile. To do that, the modelling and setup of the different geometries as well as the clarification and characterization of the physics, material properties and BCs and the analyses and discussions about the results will be necessary.

## 1.2   STRUCTURE OF THE THESIS

In the first third section of the Thesis, the theoretical foundations for practical work are explained. These include the basics of nuclear fusion and fusion devices but also concepts of heat transfer and solid mechanics. This will help setting up a link between the two and allow building and propose a performance indicator based on positions in an operational space to validate proper functioning.

The second and the third sections, the methods and models as well as the results and the discussions of the analyses will be done and concluded at the very end of this work.

## 2 | THEORETICAL FRAMEWORK

In this chapter, the basics of fusion such as nuclear physics and magnetic confinement are explained. In addition to that, the construction and the different systems of the W7-X are also explained to give an overview on the device and its auxiliary components. Heat transfer theory as well as solid mechanics including plasticity and fatigue constitute the basis of the work and the complex equations of these theories solved using Finite Element Analysis. These theories are necessary for the completion of this work and are therefore reminded in this chapter.

### 2.1 GENERAL THEORY OF FUSION REACTORS

The principle of a nuclear fusion power plant is to make the energy released by the fusion of light atomic nuclei usable. Nuclear fusion which represent the fusing of atomic nuclei together is only achievable if they come close enough to surpass the electrostatic repulsion forces and have the strong nuclear force fuse the nucleons together. Due to electrostatic repulsion forces also called Coulomb barrier, the nuclei repulse each other thus preventing the reaching of the necessary distance (because the strong nuclear force has a very limited range, $10^{-15}$ m) [2][4] for fusion. Furthermore, the repulsion forces increase with the number of protons in the nucleus or its size. The energy required to fuse two nuclei become subsequently greater.
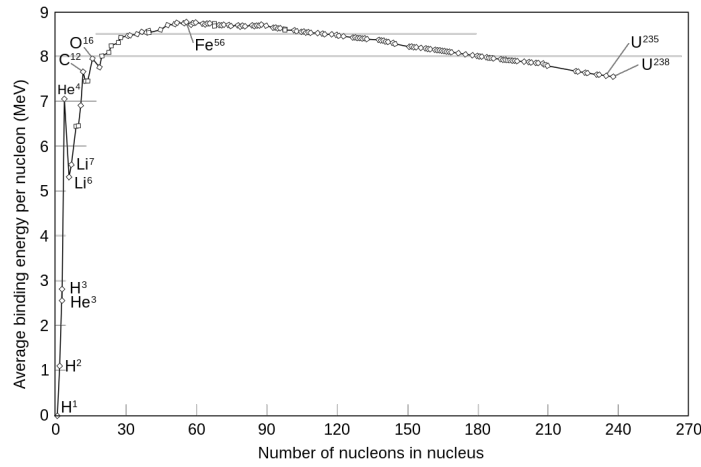


Figure 2.1: *Nuclear binding energy vs. mass number.*

The different nuclear reactions for transforming hydrogen into helium are [2]:

$$_1^1\text{H} + {_0^1}\text{n} \longrightarrow {_1^2}\text{H} + 2.22\,\text{MeV}^1 \tag{2.1}$$

$$_1^2\text{H} + {_1^1}\text{p} \longrightarrow {_2^3}\text{He} + 5.49\,\text{MeV} \tag{2.2}$$

or

$$_1^2\text{H} + {_1^2}\text{H} \longrightarrow {_2^3}\text{He} + {_0^1}\text{n} + 3.27\,\text{MeV} \tag{2.3}$$

$$_1^2\text{H} + {_1^2}\text{H} \longrightarrow {_1^3}\text{He} + {_1^1}\text{p} + 4.03\,\text{MeV} \tag{2.4}$$

$$_1^2\text{H} + {_1^3}\text{H} \longrightarrow {_2^4}\text{He} + {_0^1}\text{n} + 17.58\,\text{MeV} \tag{2.5}$$

On Figure 2.2, the cross section for various reactions are graphed in function of the ion temperature. The cross section represents the area on which it is possible for nuclei to collide and subsequently fuse together. The higher the cross section, the higher the nuclei are likely to collide with each other. For lower ion temperatures, the Deuterium-Tritium reaction has the biggest cross section. The easiest way to initiate fusion is by the Deuterium–Tritium reaction, which releases $17.6MeV$, $14.1MeV$ in the neutron and $3.5MeV$ in the alpha particle. [4]
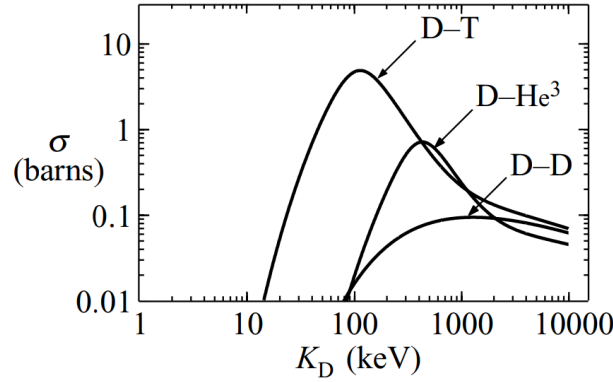
Figure 2.2: *Fusion cross sections for various fusion reactions (D-T, D-He$^3$ and D-D) versus ion temperature. [4]*

When the cross section is known, is it possible to calculate the reaction rate for the main fusion reactions. The reaction rate is noted $\langle\sigma v\rangle$. These results are illustrated in Figure 2.3 as curves of $\langle\sigma v\rangle$ vs. ion temperature $T$. It is possible to observe that the peak value of the reation rate is $9 \times 10^{-22}m^3s^{-1}$ at $70keV$ for the D-T fuel mix.
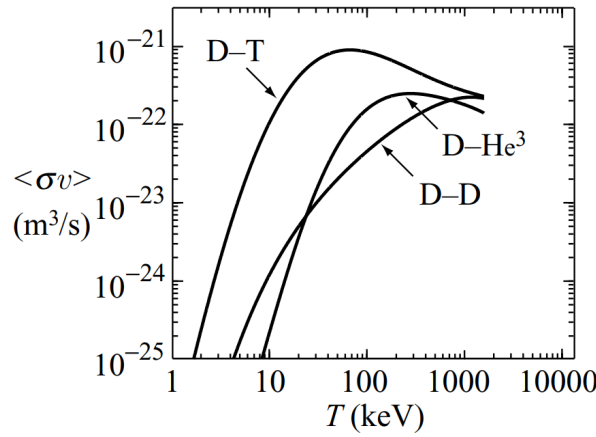
Figure 2.3: *Velocity averaged cross section $\langle\sigma v\rangle$ for various fusion reactions (D-T, D-He$^3$ and D-D) versus ion temperature. [4]*

As said previously, the energies to achieve nuclear fusion are important. One solution to this problem is to give the correct amount of kinetic energy to the nuclei in order for them to overcome the Coulomb barrier. This kinetic energy is measured in Electron-Volts and is obtained by heating the fuel to high temperatures. The temperature thus reaches 100M to 200M°C [2], which is hotter than the sun's core. At those temperatures, the fuel becomes a plasma, which is often considered as the fourth state of matter. Plasma is also called the highest state of aggregation of a substance designated. In this aggregate state, the internal energy is far higher than the binding energy between the electrons and the nuclei. This means that the electrons can move freely. Plasma differs greatly in its properties from normal gases.

The important temperature of the plasma forces various measures to be taken to ensure that the Materials built into the fusion reactor near the plasma provide maintained thermal insulation and compensate for the resulting expansion pressure. A solution to this problem is the exploiting of the Lorenz force affecting the charged particles of the plasma. The idea is, at least for magnetic confinement, to trap the plasma inside a magnetic cage. This will help levitating the plasma and control its shape and position to avoid touching any PFCs. The distance between the plasma and the PFCs is crucial since contact could generate plasma turbulence or contaminate the plasma with impurities, reducing the quality of it. Different systems where developed to build such a confinement.

There are two different type of magnetic confinement concepts that are widely know and developed, the Tokamak and the Stellarator. These two magnetic confinement devices are both based on a toroidal geometry, the difference between the two of them being the way the plasma is confined. In a Tokamak machine, the plasma is confined using planar toroidal magnetic coils. Those coils help create the toroidal magnetic field component of the confinement. Although this seems like a good confinement, other problems still need to be addresses such as the effect of particle drift. This drift is due to pressure gradients and inhomogeneities in the magnetic field inside the plasma and leads to a drift of the particles towards the outer diameter of the Tokamak. This complex particle transport phenomenon can be mitigated by introducing a poloidal component to the magnetic field, causing a rotation of the plasma around its toroidal axis. To achieve this magnetic field, Tokamaks use a solenoid coil placed at the center of the torus. This solenoid coil acts as a primary transformer coil, a time-varying electric current generate a varying magnetic field which itself induce an electric current inside the plasma. The resulting movement of charges inside the plasma generate a poloidal magnetic field, the plasma is then generating its own magnetic field. This electric current can also be used to heat up the plasma, it is called ohmic heating.
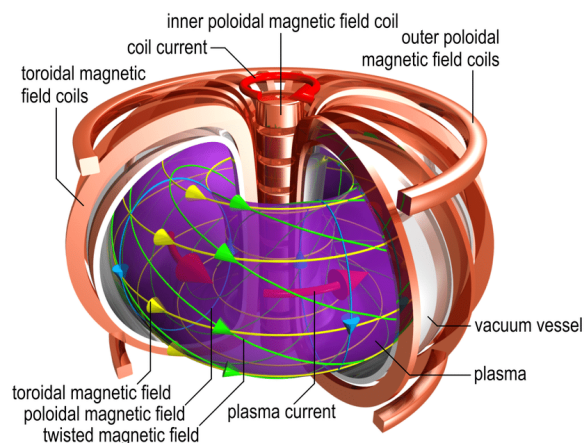


Figure 2.4: *Schematics of a Tokamak confinement, courtesy of C. Brandt*

While this solution is good, there are problems with it. The main issue is the inherently transient process. The poloidal component of the magnetic field can only be generated as long as the current in the solenoid coil varies. This means that the reactor can only run in pulses and steady-state isn't currently achievable.

Another solution for generating the poloidal magnetic field is to twirl the plasma in such a shape, that the drift phenomenon disappears. This solution is the Stellarator. The Stellarator was first introduced by Lyman Spitzer in the 1950s. This technology was put aside because of technical difficulties and because the Tokamaks presented better performances. The Stellarators use a complex set of magnets allowing to generate a precise magnetic field allowing the plasma to not experience significant drift. Contrary to Tokamaks, Stellerators plasmas don't have a plasma current. This solution also helps with confinement, as the magnetic field can be adjusted to accommodate for the strict equilibrium conditions. The absence of plasma current also means that Stellarators can be operated in steady-state since no current induction is needed, thus being more suitable for power plants. Although allowing improved plasma confinement, Stellarators are plagued by complex geometries that are often too complex to be feasible.
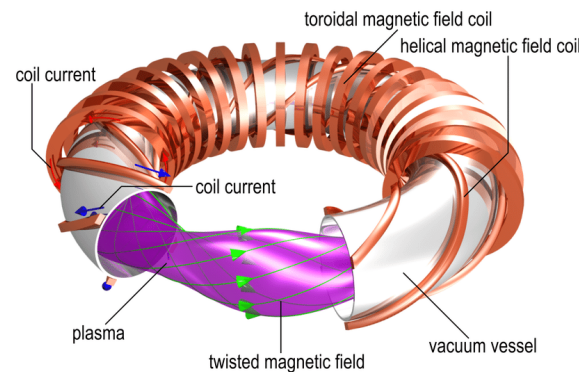


Figure 2.5: *Schematics of a Stellarator confinement, courtesy of C. Brandt*

The goal of those magnetic confinement fusion reactors concepts is to propose a new way of producing atomic energy while avoiding the drawbacks of traditional fission reactors (ie. Management of radiation, production of highly radioactive long half-life elements, limited fuel supply. . . ). Although fusion energy is attractive, many problems still need to be addresses such as tritium breeding issues or neutron transport and interaction with the structure.

## 2.2   W7-X SYSTEMS

he Wendelstein 7-X (W7-X) is a stellarator nuclear fusion experiment with a significant history that underscores its importance in fusion research. The idea for W7-X was born in the late 1980s and early 1990s, aimed at testing the viability of stellarator design for sustained fusion reactions. This project built upon the success of its predecessor, Wendelstein 7-AS.

In 1996, the German government approved the construction of W7-X, with substantial funding from the European Union and international partners. Construction began in 1997 at the Max Planck Institute for Plasma Physics (IPP) in Greifswald, Germany. This phase involved assembling complex superconducting magnetic coils and a highly precise vacuum vessel, presenting numerous technical challenges that required innovative solutions.

By 2014, the assembly of W7-X was completed, marking a major milestone. The machine produced its first plasma on December 10, 2015, demonstrating the functionality of its design and construction. Following this achievement, W7-X entered its experimental phase. Initial experiments focused on achieving and maintaining stable plasma conditions, testing heating methods, and studying plasma behavior.

Over the subsequent years, W7-X achieved several key milestones, including sustained plasma discharges lasting up to 100 seconds and significant advancements in plasma heating and density. These experiments provided valuable insights into plasma confinement and stability, moving closer to the goal of long-pulse operations lasting up to 30 minutes. This capability is critical for the development of future fusion power plants, as it demonstrates the potential of stellarators for continuous operation.

Research continues to optimize plasma performance, improve heating and control techniques, and deepen the understanding of stellarator physics. The Wendelstein 7-X remains a cornerstone of global fusion research, contributing valuable data and insights that support the broader goal of developing practical and sustainable fusion energy.

## 2.3   HEAT TRANSFER

In this section, the fundamental principles and governing equations and each heat transfer mode are explored. The TZM-reflector tile is a highly constrained mechanical part that of the HS. This part will be exposed to plasma radiation as well as the ECRH beam. The heat transfer in this system is complex and need a good understanding of the theory to model it as good as possible.

The heat loads on the ECRH reflector tile are specified further in the thesis but the theory first needs to be explained, at least what will be needed for this task.

### 2.3.1   General problem of heat exchange

Heat exchange happens all the time and everywhere in nature, from the sun's radiative power to the heat transfer on the surface of the skin. Historically, heat was considered as some sort of *flow* that would flow from one hot object to another colder object [5]. The idea of an invisible fluid flowing from a body to another called *Caloric* was first considered to explain this heat transport. While the caloric theory of heat exchange is acceptable to consider such a concept for explaining heat transport, there are more modern approaches to heat exchange that will be discussed later [5]. The general problem of heat transfer involves understanding how thermal energy is transported from one place to another. The modern aproach to heat transfer is the *kinetic* theory. Heat is defined to be the average Velocity of the particles within an system. This approach helps to understanding what heat is physically [1]. Heat exchange can be seen in many different situations and takes place in every medium and different modes. Leaving a hot house during winter with a door open and having the hot air making its way out, hummingbirds using a counterflow heat exchanger in their feet to regulate their body temperatures [6] or inadvertedly touching a hot pan are all examples of heat exchange between mediums and objects [5]. It respects some rules such as the flow direction, from hot to cold.

Not only in nature but also in industry, heat is heavily used for/or is a product of chemical processes. Steam boilers convert chemical energy into heat to generate steam and then generate elctricity, this is also true for nuclear power plants, using the heat generated by fission reactions to generate steam. Heat is generated in combustion engines and needs to be evacuated meanwhile in fridges, heat in pumped to decrease the temperature in a chamber. Those devices all use some sort of heat transfer in order to work properly. Heat exchange is also present throughout of fusion devices at many different levels such as inside the plasma as well as the first wall components and the pumping system. Correctly modelling heat exchange as well as understanding the physical phenomena behind the transfer of heat in thermal ma-

chines.

Thermodynamics is a theory about the dynamics and conversion of different energy forms heavily developed during the 19th century. It provides a very good framework in which it is possible to built a theory of heat exchange [5]. It is possible to derive the equation of heat transfer from the laws of thermodynamics. The first law of thermodynamics for a closed system, as taught in engineering programs, takes the following form:

### 2.3.2 Heat conduction

Conduction is the transfer of energy from the more energetic particles of a substance to the adjacent less energetic ones as a result of interactions between the particles [1]. Conduction can take place in solids, liquids, or gases. In fluids, conduction is due to the collision and diffusion of the molecules during their random motion. In solids, conduction is due to the combination of vibration of the molecules in a lattice and the energy transport by free electrons.

Lets consider steaty-state heat conduction through a plane wall of thickness $L = \Delta x$ and area $A$. The difference of temperature or *gradient* is measured and is written $\Delta T = T_2 - T_1$. Experience has shown that the rate of heat transfer $\dot{Q}_{cond}$ through the wall would double when the temperature gradient across the wall *or* when when the area $A$ normal to the direction of heat transfer doubles. The rate of heat transfer would be halved when the thickness $L$ doubled. Qualitavively, it is possible to conclude that the rate of heat conduction through a plane wall is proportional to the temperature gradient across the layers and the heat transfer area, but is inverssely proportional to the thickness of the layer. The relation between the quantities is:

$$(Rate\ of\ heat\ conduction) \propto \frac{(Area)(Temperature\ gradient)}{Thickness} \tag{2.6}$$

Analytically, the mathematical law describing the conduction of heat is **Fourier's law of heat conduction**. The coefficient $k$ is the thermal conductivitiy, which is the abilitiy of a certain material to conduct heat. It is possible to write this law using quantities and the equation is :

$$\dot{Q}_{cond} = -kA\frac{T_2 - T_1}{\Delta x} = -kA\frac{\Delta T}{\Delta x} \qquad [W] \quad (2.7)$$

When $\Delta x \to 0$, the one-dimensionnal differential form of the equation is written:

$$\dot{Q}_{cond} = -kA\frac{dT}{dx} \qquad [W] \quad (2.8)$$

On the left hand side of the heat conduction equation 2.8 $\dot{Q}_{cond}$ decribes the time derivative or temporal rate of change of the heat flux flowing though a surface. On the the right hand side of the equation, $k$ is the thermal conductivity. Usually, the thermal conductivity is a function of the temperature itself making this differential equation nonlinear.

### 2.3.3 Convective heat transfer

It was mentionned earlier that there are three basic mechanisms of heat transfer: conduction, convection, and radiation. Conduction and convection are similar in that both mechanisms require the presence of a material medium. But they are different in that convection requires the presence of fluid motion. Heat transfer through a solid is always by conduction, since the molecules of a solid remain at relatively fixed positions. Heat transfer through a liquid or gas, however, can be by conduction or convection, depending on the presence of any bulk fluid motion. Heat transfer through a fluid is by convection in the presence of bulk fluid motion

and by conduction in the absence of it.

#### 2.3.4  Thermal radiation
### 2.4  SOLID MECHANICS
### 2.5  FINITE ELEMENT METHOD

# 3 | STATE OF THE ART

In this chapter, the design, the use and the architecture of the reflector tile will be explained. Moreover, the already existing analyses and results will be discussed to give context and insight about the situation and the functionning of this system.

## 3.1 THE ECRH TZM REFLECTOR TILE ASSEMBLY

The reflector tile is used to reflect the ECRH beam back into the plasma to limit energy loss. This reflector tile is placed a a particular position inside of the stellarator. The reflector tiles face the plasma and are a component of the PFCs and are placed in front of the ECRH launch towers. A reflective alloy made of titanium zirconium and molybdenum abbreviated TZM was chosen to build the reflector tile. The reflector tile is mounted on a copper chromium zirconium heat sink that is brazed onto a stainless steel cooling pipe. The ECRH reflector tile is placed on one of the modules composing the in-vessel components or KiP.

INSER TEXT ABOUT MONTAGE

## 3.2 PREVIOUS ANALYSES OF THE ECRH REFLECTOR TILE

In order to reflect the ECRH beam into plasma back, some TZM tiles were suggested to substitute the BM graphite tiles in specific positions. The idea was to limit power loss due to absorption of the ECRH beam by the graphite tiles. After OP1.2 it was decided to increase the size of the TZM tile. Due to the fact the tile has been never analyzed in details, corresponding thermal and structural analysis is to be performed to assess the performance of the tile in OP2.

For OP2, plasma discharge duration will be increased thus exposing the PFCs to longer heat loads. The "worst" tile had been selected during discussion between V. Bykov and T. Stange and was analyzed. Those analyses aimed to give insight about the thermal and structural integrity of the ECRH reflector tile during the plasma discharges with OP2 specifications.

Different analyses such as transient thermal and fatigue analyses were performed by various engineers to assure proper functioning of the tile. One of those analyses were performed by J. Fellinger in 2013 and was the thermal-mechanical assessment of heat shields and baffles [3]. The analyses were performed on a simplified model *see figure* 3.1 of the tile and calculated using Dassault Systèmes Abaqus. Perfect thermal contact between the parts was also assumed to simplify the model. The heat pulse was simplified to be a step signal lasting for about 90 *s*. Models for fatigue dimensionning and material properties were defined and used in this work. Thermal properties of the differents materials used are also given and important for the rest of the work.

The conclusions of this work were that the fatigue of the steel cooling pipe.
The plastic strain in the steel pipe under test conditions remains within the acceptable limit of 0.9% for low cycle fatigue (LCF) after 500 cycles, indicating that no failure or leakage occurred during the test. However, the plastic strain significantly exceeds the 0.2% limit for 60,000 cycles as planned for W7-X.
The effect of the boundary conditions, in particular restraining the axial displacement of the the steel cooling pipe has a non-negligible and detrimental influence on the plastic strain [3]. This conclusion is going to be seen later in this work regarding the structural analysis.

In this work, a discussion about the thermal performances of the brazing between the heat sink and the cooling pipe or the Sigraflex thermal gasket also stated that these moderatly
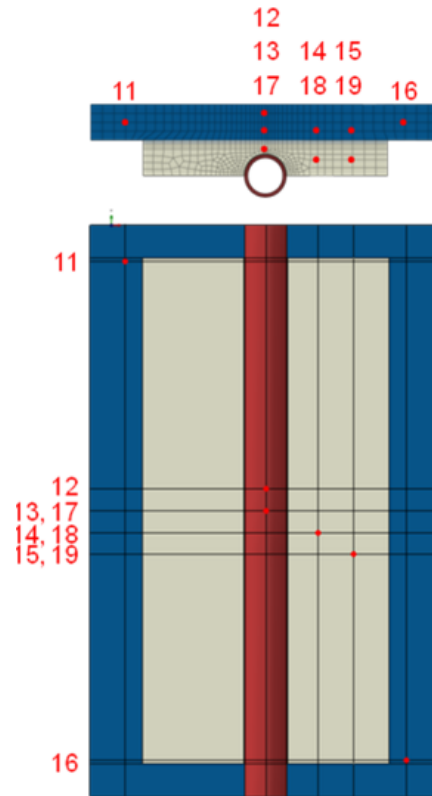
Figure 3.1: *FE model of the tile assembly [3]*

affected the heat transfer within the tile assembly. On the other hand, the annealing of alloys and the temperature-dependant mechanical properties are a concern and the issue of having uncertain annealing of the CuCrZr due to termal activation arose [3]. This will be an issue discussed later in the topic of this work.

Later, Jiawu Zhu was tasked to analyse the behavior of the tile

### 3.3   ISSUES OF THE TILE

# 4 | METHODS AND CONFIGURATIONS

As stated in the state of the art; the object of these analyses is the ECRH TZM-reflector tile (ref. E821). To study the thermal and mechanical behavior of this in-vessel component, finite element analysis using the ANSYS® software will be carried out to evaluate the new design's performances and the proposed solution to the overheating of the CuCrZr heat sink issue. Coupled physics analyses, in particular one-way coupling and full coupling of thermal and structural analyses, will be used to assess the effects of the design changes and validate the proper functioning of the reflector tile in OP2 design loads.

## 4.1 MATERIAL PROPERTIES AND PHYSICAL MODELS

One of the crucial point of this task are the material properties such as the thermal and mechanical properties and behavior. Those properties can have a big influence on the results of the calculations and they need to be carefully set to accurately model the real life metarial. As is in real life, the material properties are often nonlinear, adding complexity to the calculations.

The first set of material properties used in early analyses were the ones used by J. Zhu in his 2019 parametric analyses [7] of the ECRH reflector tile. The properties included the ones for:

- Titanium Zirconium Molybdenum for the reflector tile.

- Copper Nickel Zirconium for the heat sink.

- Stainless Steel 1.4981 $X8CrNiMoNb$ for the cooling pipe.

- Sigraflex for the thermal gasket between the heat sink and the reflector tile.

A few of these material properties were based on outdated sources and needed reevalutation to take into account any change.
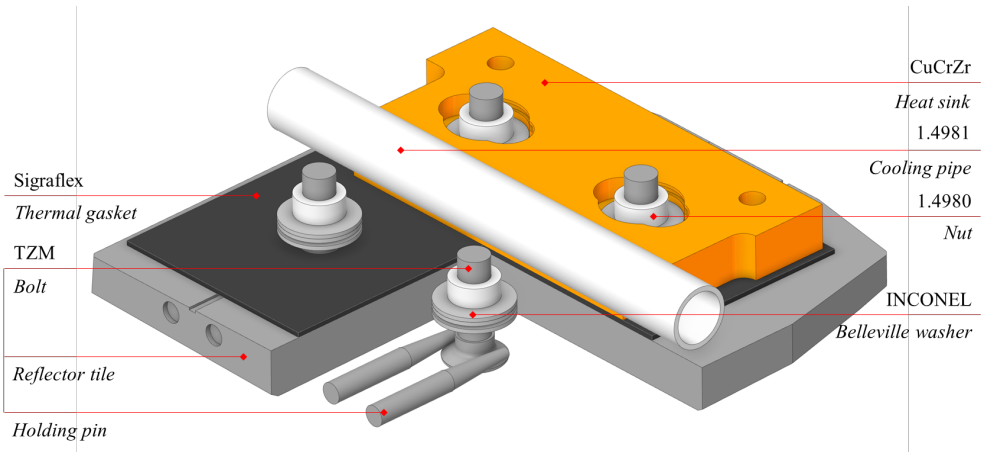


Figure 4.1: *Material assignation*

The new material properties were set during the project and are split into two big categories, the thermal/physical properties and the mechanical properties. This new set was then saved in an *.xml* file to be ported to other ANSYS Workbench® projects (ie. thermal-structural analysis of Neutral Beam Injection target tile).

### 4.1.1 Thermal properties

Thermal analysis is the main type of analysis done to evaluate the performances and behavior of the TZM reflector tile and tile assembly. This is why an accurate modelling of the assembly's constitutive materials is crucial. In addition to the first four materials, the new model should implement the bolting system comprised of TZM bolts and holding pins, 1.4980 *X5NiCrTi* SS nuts and 2.4668 Inconel Belleville washers. The bolting system was not included in the 2019 model of J. Zhu [7]. Understanding the impact of such bolting system is important to fully analyse the tile. The complete list for thermal properties is (after update):

- Titanium Zirconium Molybdenum for the reflector tile, bolts and holding pins

- Copper Nickel Zirconium for the heat sink.

- Stainless Steel 1.4981 *X8CrNiMoNb* for the cooling pipe.

- Sigraflex for the thermal gasket between the heat sink and the reflector tile.

- Stainless Steel 1.4980 *X5NiCrTi* for the nuts.

- 2.4668 Inconel for the Belleville washers.

It is also important to note that phenomena such as thermal activation and recrystallization of the alloys are NOT taken into account although finite element analysis could technically support such calculations. The implementation of such physical phenomena would require more material data and more ressources in order to correctly model them. It was simply decided to avoid (*if possible*) reaching the recrystallization temperatures of the different part material (in particular the maximum temperature of the CuCrZr heat sink since it is the part that was would overheat [7, 3]).

### 4.1.2 Mechanical properties

Mechanical analysis is the second analysis type that will be carried out to evaluate the structural integrity of the reflector tile assembly. Structural analyses are more complex than thermal analyses and require most computing power. They also heavily depend on the meshing and the modelling of the material (ie. plasticity, elasticity) can greatly influence the results. This is why the choice of the material model is pertinent. In his 2019 study, J. Zhu analyzed the fatigue cycle of the reflector tile assembly [7]. The fatigue criteria will not be used in this study.

Hardening and plasticity of the material will only be used in special cases (notably for the CuCrZr alloy) to assess the plastic deformation of the parts. For most, the hardening law will be perfectly plastic (tangent modulus = 0 [*GPA*]) and it was assumed (as a first approach) that the parts shouldn't deform plastically.

After reading different datasheets and suppliers data, the mechanical properties were reevaluated and condensed into a new revised material database. For the Stainless Steel 1.4981 *X8CrNiMoNb* of the cooling pipe, the mechanical properties were not given and another similar alloy, in particular 1.4435, was used for its mechanical properties ONLY. For other materials such has Sigraflex, the material data was very limited for lack of supplier's data of a better characterization of it.

The updated thermal and mechanical properties of the materials are given in tables.

| $T$ | $\lambda$ | $\alpha$ | $C_p$ | $E$ | $\nu$ | $\rho$ |
|---|---|---|---|---|---|---|
| $[°C]$ | $[W\,m^{-1}°C^{-1}]$ | $[°C^{-1}]$ | $[J\,kg^{-1}°C^{-1}]$ | $[GPa]$ | $-$ | $[kgm^{-3}]$ |
| 20 | - | 5,30E-06 | - | 300 | 0,32 | 10200 |
| 25 | 122 | - | 248 | - | - | - |
| 100 | 121 | - | 255 | - | - | - |
| 200 | 119 | 5,30E-06 | 264 | - | - | - |
| 400 | 116 | 5,40E-06 | 279 | - | - | - |
| 500 | - | - | - | 260 | 0,32 | - |
| 600 | 112 | 5,60E-06 | 289 | - | - | - |
| 800 | 109 | 5,80E-06 | 299 | - | - | - |
| 1000 | - | 6,00E-06 | - | 220 | 0,32 | - |
| 1200 | - | 6,20E-06 | - | - | - | - |
| 1400 | - | 6,40E-06 | - | - | - | - |
| 1500 | - | - | - | 140 | 0,32 | - |
| 2000 | - | - | - | 40 | 0,32 | - |

Table 4.1: Thermal and mechanical properties of Titanium Zirconium Molybdenum

| $T$ | $\lambda$ | $\alpha$ | $C_p$ | $E$ | $\nu$ | $\rho$ |
|---|---|---|---|---|---|---|
| $[°C]$ | $[W\,m^{-1}°C^{-1}]$ | $[°C^{-1}]$ | $[J\,kg^{-1}°C^{-1}]$ | $[GPa]$ | $-$ | $[kgm^{-3}]$ |
| 20 | 338 | 1,57E-05 | 388 | 128 | 0,3 | 8920 |
| 100 | 342 | 1,63E-05 | 392 | 125 | 0,3 | - |
| 200 | 350 | 1,70E-05 | 400 | 121 | 0,3 | - |
| 300 | 360 | 1,76E-05 | 410 | 115 | 0,3 | - |
| 400 | 372 | 1,82E-05 | 422 | 109 | 0,3 | - |
| 500 | 387 | 1,86E-05 | 437 | 102 | 0,3 | - |
| 600 | 404 | 1,88E-05 | 454 | - | - | - |
| 700 | 423 | 1,90E-05 | 473 | - | - | - |

Table 4.2: Thermal and mechanical properties of Copper Nickel Zirconium

| $T$ | $\lambda$ | $\alpha$ | $C_p$ | $E$ | $v$ | $\rho$ |
|---|---|---|---|---|---|---|
| $[°C]$ | $[W\ m^{-1}°C^{-1}]$ | $[°C^{-1}]$ | $[J\ kg^{-1}°C^{-1}]$ | $[GPa]$ | $-$ | $[kgm^{-3}]$ |
| 20 | 13,5 | 1,61E-05 | 472 | 196 | 0,3 | 8010 |
| 100 | 14,9 | 1,67E-05 | 501 | 190 | 0,3 | - |
| 200 | 16,7 | 1,72E-05 | 525 | 182 | 0,3 | - |
| 300 | 18,3 | 1,77E-05 | 532 | 174 | 0,3 | - |
| 400 | 19,8 | 1,81E-05 | 555 | 166 | 0,3 | - |
| 500 | 21,3 | 1,84E-05 | 582 | 158 | 0,3 | - |
| 600 | 22,7 | 1,88E-05 | 604 | 150 | 0,3 | - |
| 700 | 24,2 | 1,91E-05 | 610 | 142 | 0,3 | - |
| 800 | 25,6 | 1,94E-05 | 611 | 134 | 0,3 | - |
| 900 | - | 1,97E-05 | 615 | - | - | - |
| 1000 | - | 2,00E-05 | 641 | - | - | - |

Table 4.3: Thermal and mechanical properties of Stainless Steel 1.4981

| $T$ | $\lambda$ | $\alpha$ | $C_p$ | $E$ | $v$ | $\rho$ |
|---|---|---|---|---|---|---|
| $[°C]$ | $[W\ m^{-1}°C^{-1}]$ | $[°C^{-1}]$ | $[J\ kg^{-1}°C^{-1}]$ | $[GPa]$ | $-$ | $[kgm^{-3}]$ |
| 20 | 15 | 1,70E-05 | 460 | 211 | 0,3 | 8000 |
| 100 | - | 1,70E-05 | - | 206 | 0,3 | - |
| 200 | - | 1,75E-05 | - | 200 | 0,3 | - |
| 300 | - | 1,78E-05 | - | 192 | 0,3 | - |
| 400 | - | 1,80E-05 | - | 183 | 0,3 | - |
| 500 | - | 1,82E-05 | - | 173 | 0,3 | - |
| 600 | - | 1,85E-05 | - | 162 | 0,3 | - |

Table 4.4: Thermal and mechanical properties of Stainless Steel 1.4980

| $T$ | $\lambda$ | $\alpha$ | $C_p$ | $E$ | $\nu$ | $\rho$ |
|---|---|---|---|---|---|---|
| $[°C]$ | $[W\ m^{-1°}C^{-1}]$ | $[°C^{-1}]$ | $[J\ kg^{-1°}C^{-1}]$ | $[GPa]$ | $-$ | $[kgm^{-3}]$ |
| 20 | 12 | 1,34E-05 | 440 | 199 | 0,31 | 8200 |
| 100 | 13 | - | - | 195 | 0,31 | - |
| 200 | - | 1,34E-05 | - | 190 | 0,31 | - |
| 300 | - | 1,38E-05 | - | 185 | 0,31 | - |
| 400 | - | 1,41E-05 | - | 179 | 0,31 | - |
| 500 | 19 | - | - | 174 | 0,31 | - |
| 600 | - | 1,47E-05 | - | 167 | 0,31 | - |
| 700 | 23 | - | - | 163 | 0,31 | - |
| 800 | - | 1,64E-05 | - | 149 | 0,31 | - |
| 900 | 27 | - | - | 134 | 0,31 | - |
| 1000 | - | - | - | 120 | 0,31 | - |
| 1100 | - | - | - | 100 | 0,31 | - |

Table 4.5: Thermal and mechanical properties of INCONEL 2.4668

| $T$ | $\lambda_X$ | $\lambda_{Y,Z}$ | $\alpha_X$ | $\alpha_{Y,Z}$ | $C_p$ | $E$ | $\nu$ | $\rho$ |
|---|---|---|---|---|---|---|---|---|
| $[°C]$ | $[W\ m^{-1°}C^{-1}]$ | $[W\ m^{-1°}C^{-1}]$ | $[°C^{-1}]$ | $[°C^{-1}]$ | $[J\ kg^{-1°}C^{-1}]$ | $[GPa]$ | $-$ | $[kgm^{-3}]$ |
| 20 | 3 | 154 | 3,00E-05 | 1,00E-06 | 700 | 0,7 | 0,15 | 1000 |
| 250 | 2,6 | 105 | - | - | - | - | - | - |
| 500 | 2,1 | 82 | - | - | - | - | - | - |
| 750 | 2,1 | 69 | - | - | - | - | - | - |
| 1000 | 2,1 | 61 | - | - | - | - | - | - |
| 1250 | 2,1 | 56 | - | - | - | - | - | - |
| 1500 | 2,1 | 53 | - | - | - | - | - | - |
| 2000 | 2,1 | 51 | - | - | - | - | - | - |

Table 4.6: Thermal and mechanical properties of Sigraflex

### 4.2   CONTACT CONFIGURATION

The ECRH TZM reflector tile is an assembly composed of different parts held together using a specific bolting system. It is crucial to correctly set the contacts of the parts to accurately model the real life phenomena. Contacts are a quite complex concept and introduce lots of different problematics when modelling them. They can have all sorts of properties such as the number of degrees of freedom and possible movement or a specific heat transfer coefficient. In the case of the reflector tile assembly, the contact are of different types, mainly unidirectional and bonded.

Mathematically, contacts such as unidirectional contacts introduce discontinuities and nonlinearities that can influence convergence of the calculations. The methods chosen for the contacts will impact the speed and stability of the calculations, this is why the settings of the contacts were chosen with great care to avoid faulty calculations and improbable results.

In real life, the TZM tile is placed on top of the Sigraflex thermal gasket. The Cu-CrZr heat sink is placed in the other side of the Sigraflex thermal gasket. Those two contacts (tile/thermal gasket and thermal gasket/heat sink) are all unidirectional and frictional. The SS cooling pipe is brazed onto the CuCrZr heat sink. This bonds the heat sink and the cooling pipe together. For this contact, it is assumed that both are thermally perfectly bonded, meaning that the temperature on one part at the boundary is the same as the temperature on the contact boundary of the other part. In some cases, this brazed contact will have a reduced contact area to simulate a "bad" brazing and assess the impact of a worsen thermal contact.

The bolting system is a complex assembly and interacting parts composed of the TZM bolts, the TZM holding pins, the SS nut, the INCONEL Belleville washers. The reflector tile has a closed plasma-facing surface. The bolts thus need to the held in the tile, and because it is not possible to directly use the reflector tile to fix the bolt. It was decided to design TZM holding pins screwed on the side of the reflector tile. Those holding/retaining pins are designed to retain the head of the bolt using fingers. In total, 8 of such pins are assembled in the reflector tile. The holding pin/reflector tile connection is threaded but it was deemed acceptable to consider it bonded. The contact between the holding pins and the bolts are, however, unidirectional and frictional. The contact nut to bolt is also threaded but is considered bonded in the model. To accomodate for possible thermal expansion and deformation of the parts while still assuring thermal contact between the TZM reflector tile and the Cu-CrZr heat sink, as stack composed of three INCONEL Belleville washers acting as a spring, putting pressure on the reflector tile and maintaining thermal contact. The washers push on the CuCrZr heat sink. All those contacts (nut/washer, and washer/heat sink) are considered to be unidirectional and frictional. The contact washer to washer is technically frictional but for modelling and solving reasons, they will be bonded at the outer perimeter, they still can rotate but not move.

#### 4.2.1   Initial contact setup

Initially, the early calculations only included (all contacts bonded):

- The TZM tile

- The Sigraflex thermal gasket.

- The CuCrZr heat sink.

- The SS cooling pipe.

This was done to test the modelling of the tile assembly and the bonding of the parts together. While this wasn't the most accurate model, the thermal claculations didn't need and more complex setup, and for the initial calculations, heat transfer was assumed to be perfect. The idea was then to add the bolting system. This means that the complex mechanical interaction between the boltins parts, especially the stack of Belleville washers needed to be modelled. A global assembly model was thus developed to implement the bolting system on the nature

of the contacts and the modelling choices stated earlier.

It is now possible to establish a contact model for the whole assembly:
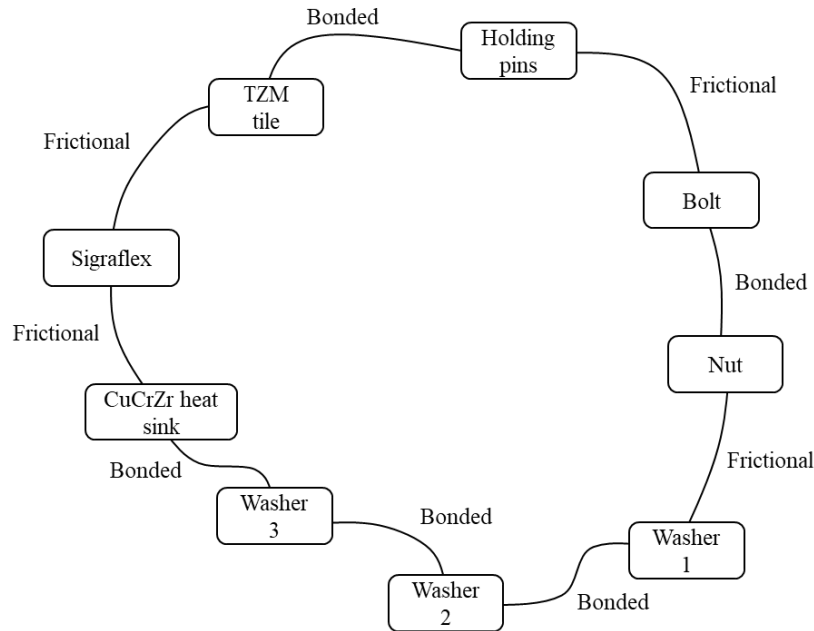


Figure 4.2: *Contact configuration for thermal and structural analysis*

This model is acceptable but will be sometimes modified to assess the impact of the contact modelling.

When setting up the contacts in ANSYS®, it is important to check for gaps of penetrations to avoid clipping issues. The status of the contact on a flat surface to surface contact should be consistent to avoid solving issues.
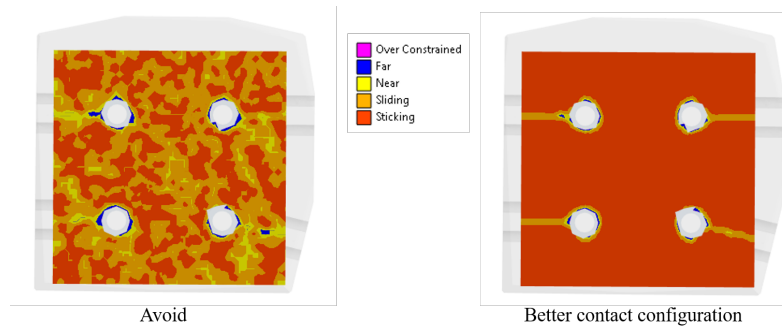


Figure 4.3: *Contact status comparison*

Such inconsistent contacts can make the calculation unstable and potentially prevent

good results. Contact offset can be used to *"close"* the gap of the contacts allowing a better contact onfiguration. Contact methods can also be modified to other formulations all having their own use cases. For bonded contact and frictional contact, programmed controlled is most used. MPC can also be used for bonded contact, it usually blocks all degrees of freedom using constrain equations. Thermal contact is considered perfect because of the brazing. It is assumed that the heat conduction is really high and the modelling is not possible without data.

### 4.2.2   Field coupling and contact configuration

Contact are complex phenomena that can be dependant on multiples fields. In the case of thermal-structural analysis, temperature and displacement fields can have an influence on the contact status of a given contact (ie. the break of contact preventing heat conduction). In chapter 5.4, field coupling is used to model the loss of contact between the heat sink and the Sigraflex. It is discussed how manual update of the contact configuration can be of use to assess the need for full field coupling. In the case of too complex

For coupled field calculations (ie. thermal-structural), the elements used have more degrees of freedom (in this case these are displacement and temperature). The problem becomes large and convergence issues arise. It was decided to remove the bolting system as a first approach. The bonding of the Sigraflex thermal gasket and the CuCrZr heat sink was done in order to simplify the model and allow better if not convergence at all.

### 4.3   PLASMA HEAT LOAD

The main heat load on the ECRH reflector tile is the plasma heat load. This reflector tile is directly exposed to the plasma. The magnitude of the thermal load depends greatly on the position of the components relative to the plasma. Components in direct contact with the plasma boundary, such as the divertor targets are loaded primarily through convected power loads, whilst the other components such as the wall panels are primarily loaded by radiation from the plasma. For the design of the PFCs it is important to know for the different plasma scenarios how the heating is split between the different components and how it is divided between convected and radiated fractions. In addition to the plasma heat load, the ECRH beam will also contribute to a certain amount to the heating of the tile assembly. Because this assembly going to be under high functionnal heat loads, it is important to correctly model the heat load of the plasma on the ECRH reflector tile.

Stationary operation, envisaged at W7-X, demands an actively cooled wall protection system. The design of the approximate 115 $m^2$ wall protection depends mainly on the distance of the last closed flux surface to the plasma facing components. The area of the outboard part, where expected heat loads do not exceed 100 ˘ 200 $kW/m^2$ will be mainly covered with actively cooled stainless steel panels (approximately 70 m2). For the rest, in particular on the inboard side, where the plasma-wall distance is smaller, higher heat loads are expected (up to 0.5 MW/m2). In this area (*about* 45 $m^2$) graphite tiles clamped on watercooled CuCrZr structures, will protect components behind the heat shield.

To respect OP2 operational and to stay consistant with the previous calculations, the value of 250 $kWm^{-2}$

### 4.4   MODELLING OF THE ECRH BEAM

One of the most crucial aspect of this task is the modelling of the ECRH beam. The correct modelling of this beam will help accurately model the real-life stray radiation of the beam.

### 4.4.1 Calculation of the integration coefficients

The issue was in the parameters of the ECRH beam load distribution since it was not clearly defined in the recalculation task requested by Torsten Stange. The little information about the parameters of the beam load were the nominal total heat flow of 912W, Gaussian shape of power distribution and the geometric properties of both axisymmetric and non-axisymmetric distribution. Based on these data, a series of calculations aiming to recalculate the load distribution on the tile surface were undergone and provided good results.
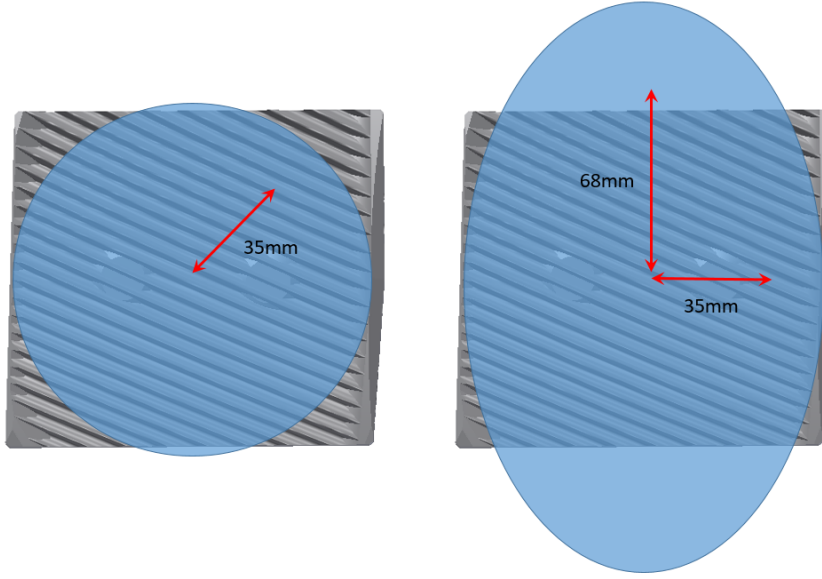


Figure 4.4: *Representation of the two ECRH beam heat flux distribution cases*

The calculation of the integral parameters as well as the analytical calculation of the surface integrals were done on Wolfram Mathematica®. There are two different cases, one axisymmetric (circular) and another non-axisymmetric (elliptical). For the first case, almost all of the power 99% hits the ECRH reflector tile. The standard deviation is defined to be 35mm, for debug and validation purposes, 86% of the power should be included within a disk of radius 35mm. For the elliptical distribution, much less power hits the reflector tile. The distribution properties are also different and feature two different radii, the minor semi-radius and the major semi-radius. Their values are respectively 35mm and 68mm, both of them defining an ellipse. Similarly to the circular distribution, for debugging, 86% of the overall power should be included within the area of the ellipse.

With help of those information, the integration coefficients could be calculated. The first integral was expressed in a cylindrical coordinate system. The first APDL code written by J. Zhu [7] in 2019 only featured the circular heat flux distribution and was based on calculations made by Torsten Stange. The integrated function for Gaussian distribution has the form $\exp(-2r^2)$. The surface integral can be written:

$$\int_\Omega \exp(-2r^2) \, dS \tag{4.1}$$

in cylindrical coordinates, $dS = r\,dr\,d\theta$ and $\Omega$ a surface in $\mathbb{R}^2$. When taking the normal distribution, is it possible to rewrite the function and include the standard deviation $r_0$. The integral $\mathbb{I}$ of $f$ on $\Omega$ is:

$$\mathbb{I}_{\Omega}^{f} = \int_{\Omega} \exp\left(-2\left(\frac{r}{r_0}\right)^2\right) dS \tag{4.2}$$

When developing the differential (in cartesian coordinates), the integral becomes:

$$\int_{\Omega} \exp\left(-2\left(\frac{r}{r_0}\right)^2\right) dS = \int_0^{+\infty}\int_0^{2\pi} \exp\left(-2\left(\frac{r}{r_0}\right)^2\right) r\,dr\,d\theta \tag{4.3}$$

$$\int_0^{+\infty}\int_0^{2\pi} \exp\left(-2\left(\frac{r}{r_0}\right)^2\right) r\,dr\,d\theta = \int_0^{+\infty} \exp\left(-2\left(\frac{r}{r_0}\right)^2\right) r\,dr \int_0^{2\pi} d\theta \tag{4.4}$$

$$= 2\pi \int_0^{+\infty} \exp\left(-2\left(\frac{r}{r_0}\right)^2\right) r\,dr \tag{4.5}$$

When calculated, the value of this integral is:

$$2\pi \int_0^{+\infty} \exp\left(-2\left(\frac{r}{r_0}\right)^2\right) r\,dr = 6,125 \cdot 10^{-4}\pi \tag{4.6}$$

This function is then normalized by multiplying both side by a coefficient $k_{norm}$ such as $k_{norm} \cdot 6,125 \cdot 10^{-4}\pi = 1$ This coefficient has a value of $519,69\ m^{-2}$. Since heat flux is in $[Wm^{-2}]$, $k_{norm}$ needs to be in $[m^{-2}]$. To validate the normalization, it is possible to integrate the same function, but only for the radius between 0 and standard deviation and multiplying the function by $k_{norm}$. This gives:

$$k_{norm}\left[\int_0^{r_0}\int_0^{2\pi} \exp\left(-2\left(\frac{r}{r_0}\right)^2\right) r\,dr\,d\theta\right] = 0,8646 \tag{4.7}$$

The integral power of the ECRH beam is 912 W. This means that normalized ECRH beam power distribution can be multiplied by the integral power. It is thus possible to define $q_0 := P_{ECRH}^{beam} \cdot k_{norm}$. In the case of the circular ECRH Gaussian heat flux distribution, the value of $q_0 = 473957\ Wm^{-2}$, this value will be used in the APDL code. The implemented function is, in cylindrical coordinates (4.9):

$$f_{axisym.}^{cyl.CS}(r) = P_{ECRH}^{beam}k_{norm}\exp\left(-2\left(\frac{r}{r_0}\right)^2\right)\ [W/m^2] \tag{4.8}$$

$$f_{axisym.}^{cyl.CS}(r) = 473957\exp\left(-2\left(\frac{r}{35[mm]}\right)^2\right)\ [W/m^2] \tag{4.9}$$

For the cartesian coordinates, the method of normalization is analog to the method used for the integral normalization in cylindrical coordinates. The choice of the cartesian coordinate system is because of the function for the elliptical ECRH power distribution case and the way the ellipse is defined. Although it is possible to vary the radius in function of the angle while working in cylindrical coordinates, or use the ellipse equation and application of Fubini's theorem in cartesian coordinates, another more practical approach was used to

compute the integral. The function $f$ written in cartesian coordinates is as follows ($a$ is the minor semi-radius and $b$ is the major semi-radius):

$$f(x,y) = \exp\left(-2\left(\left(\frac{x}{a}\right)^2 + \left(\frac{y}{b}\right)^2\right)\right) \tag{4.10}$$

The integral of the function over $\Omega$ is written:

$$\mathbb{I}_\Omega^f = \int_\Omega \exp\left(-2\left(\left(\frac{x}{a}\right)^2 + \left(\frac{y}{b}\right)^2\right)\right)\, dS \tag{4.11}$$

in cartesian coordinates, $dS = dxdy$ and $\Omega$ a surface in $\mathbb{R}^2$. For the moment, the function (4.10) is integrated over $\mathbb{R}^2$. To normalize the integral, it is possible to proceed the same way than for the cylindrical integral (4.2).

$$\int_{\mathbb{R}^2} \exp\left(-2\left(\left(\frac{x}{a}\right)^2 + \left(\frac{y}{b}\right)^2\right)\right)\, dS = \int_{-\infty}^{+\infty}\int_{-\infty}^{+\infty} \exp\left(-2\left(\left(\frac{x}{a}\right)^2 + \left(\frac{y}{b}\right)^2\right)\right)\, dxdy \tag{4.12}$$

If $a$ and $b$ are equal, the distribution is circular. The normalization coefficient for the cartesian should therefore be the same as the cylindrical one since the standard deviation of the distribution is the same, the function is just expressed in a cartesian coordinate system. Let $a = b = 35mm$, the integral becomes:

$$\int_{-\infty}^{+\infty}\int_{-\infty}^{+\infty} \exp\left(-2\left(\frac{x+y}{35[mm]}\right)^2\right)\, dxdy = 6,125\cdot 10^{-4}\pi \tag{4.13}$$

The normalization coefficient is $519,69\ m^{-2}$ and the integration coefficient $q_0 = 473957\ Wm^{-2}$. This coefficient is the same as the one for the distribution expressed a cylindrical coordinates. To validate this, it possible to proceed the same as with the cylindrical distribution, integrating over a disk of radius 35 $mm$. There is a problem with integrating the function on a circle in Cartesian coordinates, because the surface is a square of a rectangle. It is however possible to find an alternative solution to this problem using the Heaviside step function. The 2D-Heaviside step function is a discontinuous function defined as follows:

$$H_\Omega(x,y) = \begin{cases} 1 & \text{if } (x,y) \in \Omega \\ 0 & \text{if } (x,y) \in \mathbb{R} \setminus \Omega \end{cases} \tag{4.14}$$

The idea to calculate the integral over a circle or an ellipse is to multiply the integrated function by the Heaviside function (4.14) to project its values over a non-zero area defined by $\partial\Omega$, the closed perimeter of the surface.

The domain on which it is necessary to integrate is bounded by the circle equation $x^2 + y^2 = r_0^2$. Because the domain is a disk, the equation becomes $x^2 + y^2 \leq r_0^2$. The domain of the circle is thus $\Omega = \{(x,y) \in \mathbb{R}^2, r_0 \in \mathbb{R} : r_0^2 - x^2 - y^2 \geq 0\}$ and by the way the Heaviside step function (4.14) is defined in Wolfram Mathematica®, it becomes $H(r_0^2 - x^2 - y^2)$.

To validate the coefficient $k = 519,69\ m^{-2}$, it is possible to now integrate in Cartesian coordinates but on a disk. As said previously, the idea is to project the values of a function $f$ on a non-zero area $\Omega$ defined by $H_\Omega$, this is written as follows:

$$\int_{\Omega_{cyl}} f\ rdrd\theta = \int_{\Omega_{car}} \langle f, H_\Omega \rangle\ dxdy \tag{4.15}$$

with $\Omega_{cyl}$ being the cylindrical integration limits and $\Omega_{cyl}$ the cartesian integration limits. The fully written and calculated integral is :
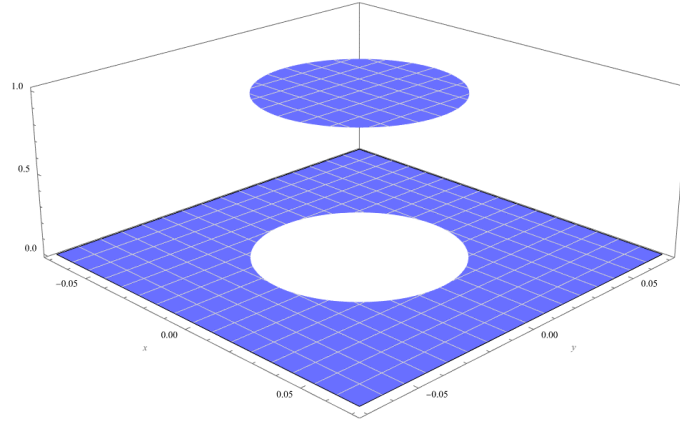
Figure 4.5: *3D graph of the Heaviside step function defined over $\Omega$*

$$k \int\limits_{-a}^{a} \int\limits_{-b}^{b} \left\langle \exp\left(-2\left(\frac{x+y}{35[mm]}\right)^2\right), H(35[mm]^2 - x^2 - y^2) \right\rangle dxdy = 0,867 \qquad (4.16)$$

The value of the integral is correct, and the integration coefficient for the Cartesian coordinates heat flux distribution is $q_0 = 473957 \, Wm^{-2}$, which is the same as the cylindrical one. This is a good sight since the distribution are defined to be the same, it is reassuring to get the same result. For the elliptical one, the method is the same as the circular one except the argument in the Heaviside step function (4.14) isn't derived for the circle equation but from the ellipse equation. The function for axisymmetric heat flux distribution written in cartesian coordinates is (4.17):

$$f_{axisym.}^{car.CS}(x,y) = 473957 \exp\left(-2\left(\frac{x+y}{35[mm]}\right)^2\right) [W/m^2] \qquad (4.17)$$

For the calculation of the non-axisymmetric integration coefficient (semi-minor radius of 35 *mm* and semi-major radius of 68 *mm*), it is possible to proceed the same way as above. The ellipse is defined via the ellipse equation $(\frac{x}{a})^2 + (\frac{y}{b})^2 = 1$ with $a$ and $b$ being respectively the minor semi-radius and major semi-radius. The Heaviside step function (4.14) is written $H\left(1 - \left(\frac{x}{a}\right)^2 - \left(\frac{y}{b}\right)^2\right)$. The normalization of the integral as well as the calculation of the integral on the ellipse is done the same way as before. The function on which the distribution $f$ is projected is the Heaviside step function (4.14) defined on an ellipse. The projection $\langle f, H_\Omega \rangle$ is integrated and the results yields a normalization coefficient $k_{norm}$ of $267,5 \, m^{-2}$ and an integration coefficient $q_0$ of $243948 \, W/m^2$. The function for non-axisymmetric heat flux distribution written in cartesian coordinates is (4.18):

$$f_{non-axisym.}^{car.CS}(x,y) = 243948 \exp\left(-2\left(\left(\frac{x}{35[mm]}\right)^2 + \left(\frac{y}{68[mm]}\right)^2\right)\right) [W/m^2] \qquad (4.18)$$

All integration coefficients as well as the standard deviations of the distributions are summarized below:

| *Loadcases* | *Integration coefficient* | $k_{norm}$ | *Semi − minor axis* | *Semi − major axis* |
|---|---|---|---|---|
| – | $[W\ m^{-2}]$ | $[m^{-2}]$ | $[m]$ | $[m]$ |
| *Axisymmetric heat flux distribution* [cyl. CS] | 473957 | 519,69 | 0,035 | 0,035 |
| *Axisymmetric heat flux distribution* [car. CS] | 473957 | 519,69 | 0,035 | 0,035 |
| *Non − axisymmetric heat flux distribution* [car. CS] | 243948 | 267,5 | 0,035 | 0,068 |

Table 4.7: ECRH beam gaussian distribution parameters

### 4.4.2   Coding strategy and implementation in ANSYS®

In ANSYS® Mechanical, the heat flux applies a uniform heat load over the whole boundary. This, of course, could be used to model the ECRH beam on the TZM tile plasma facing surfaces. While possible, this would be too conservative for the results and provide unrealistic data. This is why, a custom heat load is used to model the heat distribution of the ECRH beam. ANSYS® Mechanical does feature an APDL command function that creates an APDL environment where it is possible to write a script that is executed when needed.
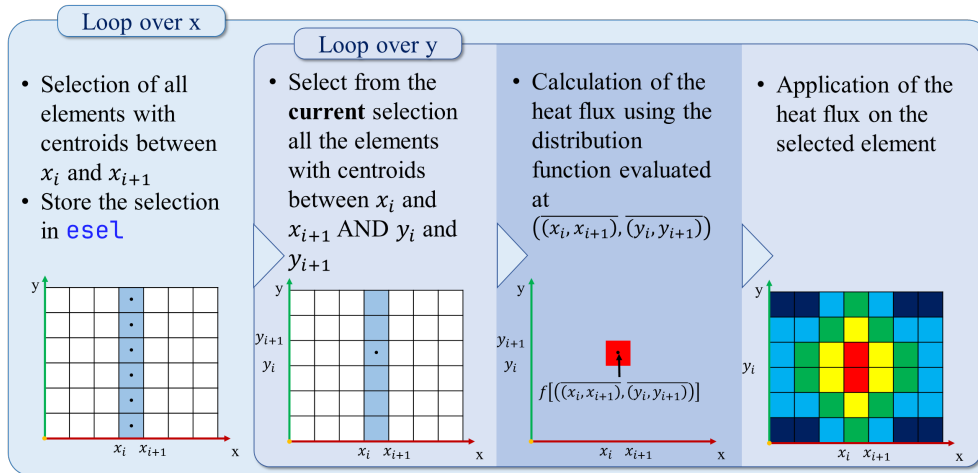


Figure 4.6: *Heat flux distribution script for APDL*

This figure shows how the cartesian code works, the original code was written in a cylindrical coordinate system.

After calculating the ECRH beam load distribution function for different cases, the functions need to be implemented in ANSYS®. The code written by J. Zhu [7] in 2019 can be reused and modified to accommodate for coordinate system change. The original code was written in cylindrical coordinates with only one loop for one variable, the radius *r*. However, the future code should support both axisymmetric and non-axisymmetric distributions, which means having two variables, *x* and *y*. First, the code calculated the heat flux following the heat flux distribution functions at the midpoint of this area (4.17)(4.18). The code then selects all elements within a small area and apply to all of them the value of the calculated heat flux from the midpoint of this area.

**Listing 1: APDL script of the gaussian heat distribution developed by J. Zhu [7]**

```
csys,100                                               1
cmsel,s,plasma_srf                                     2
esln                                                   3
esel,r,ename,,152                                      4
nsle                                                   5
cm,temp,elem                                           6
                                                       7
cycn=arg3/arg2+1                                       8
cycn=nint(cycn)                                        9
                                                       10
!--------------------------------!                     11
*do,n_,1,cycn !positive                                12
    cmsel,s,temp                                       13
    x1=(n_-1)*arg2                                     14
    x2=n_*arg2                                         15
    x0=(x1+x2)/2                                        16
                                                       17
    esel,r,cent,x,x1,x2                                18
    *get,elemn_,elem,0,count                           19
                                                       20
    !calc the heat flux follow the above formula       21
    flux_0=-2*(x0/0.05)**2                             22
    flux_x=250000*exp(flux_0)+arg1                     23
                                                       24
    *if,elemn_,ne,0,then                               25
        sfe,all,1,HFLU,1,flux_x                        26
    *endif                                             27
*enddo                                                 28
                                                       29
!--------------------------------!                     30
alls $ csys,0                                          31
                                                       32
kbc,1                                                  33
```

The code above was developed by J. Zhu for the ECRH beam implementation in ANSYS®. This code was reused to help compare the new code with the existing one. The new code below was developed to support both axisymmetric and non-axisymmetric heat load distribution. The non-axisymmetric distribution is expressed in a cartesian coodirnate system, the code should then be rewritten to include a double for-loop, one for the each axis. The new code is a little bit longer but can support any distribution. It was tested extensively by calculating the surface integral and comparing the results with the analytical calculations (*see 5.1.1*).

**Listing 2: APDL script of the gaussian heat distribution developed for both axisymmetric and non-axisymmetric**

```
csys,110                                                           1
cmsel,s,plasma_srf                                                 2
esln                                                               3
esel,r,ename,,152                                                  4
nsle                                                               5
cm,temp,elem                                                       6
                                                                   7
cycn=arg3/arg2+1                                                   8
cycn=nint(cycn)                                                    9
                                                                   10
!-------------------------------!                                  11
*do,i_,1,cycn                                                      12
    x1=(i_-2)*arg2                                                 13
    x2=(i_-1)*arg2                                                 14
    x0=(x1+x2)/2i                                                  15
                                                                   16
    *do,j_,1,cycn                                                  17
        !selection of the temperature                             18
        cmsel,s,temp                                               19
        y1=(j_-2)*arg2                                             20
        y2=(j_-1)*arg2                                             21
        y0=(y1+y2)/2                                               22
                                                                   23
        esel,r,cent,x,x1,x2                                        24
        esel,r,cent,y,y1,y2                                        25
        *get,elemn_,elem,0,count                                   26
                                                                   27
        !calc the heat flux follow the above formula              28
        flux_0=-2*((((x0-0.052067)/0.035)**2)+(((y0               29
            -0.05142)/0.068)**2))
        flux_x=243948*exp(flux_0)+arg1                             30
                                                                   31
        *if,elemn_,ne,0,then                                       32
            sfe,all,1,HFLU,1,flux_x                                33
        *endif                                                     34
    *enddo                                                         35
*enddo                                                             36
                                                                   37
!-------------------------------!                                  38
alls $ csys,0                                                      39
                                                                   40
kbc,1                                                              41
```

# 5 | ANALYSES SETUP AND RESULTS

intro to ch5

## 5.1 STEADY-STATE THERMAL ANALYSIS

Steady-state thermal analysis is the main type of analysis that was carried out to analyse the different components of the ECRH TZM-reflector tile assembly. Different scenarios and loadcases were designed to give insight on the thermal behavior and performances of the tile, that being, the impact of the design changes of the TZM-reflector tile, the influences of different ECRH beam configurations or the influences of the film coefficient in the cooling pipe.

### 5.1.1 Calculation of the surface integrales

To compare between the old and new tile design but also validate the finite element model, calculating the surface integral can be of use. This idea behind this is to check for energy conservation after integration the heat flux of the ECRH beam on the tile surface. Analytical calculations are a good approach to estimate the overall heat flow through the TZM tile. After the calculation of the surface integrales (*see* 4.4), it is possible to numerically estimate an integral and predictict the heat flux through the old and the new design.

The surface onto which the heat disribution is integrated is a rough approximation of the surface of the TZM tile (the projected area of the tile was simplified to a rectangle of size $95mm \times 95mm$). The function is then integrated using a Wolfram Mathematica® script. To evaluate the validity of the analytical calculation, a finite element model including only the old and the new TZM tile was developed to calculate the surface integral but using the finite element method. The idea is to compare both methods to estimate the heat flow.
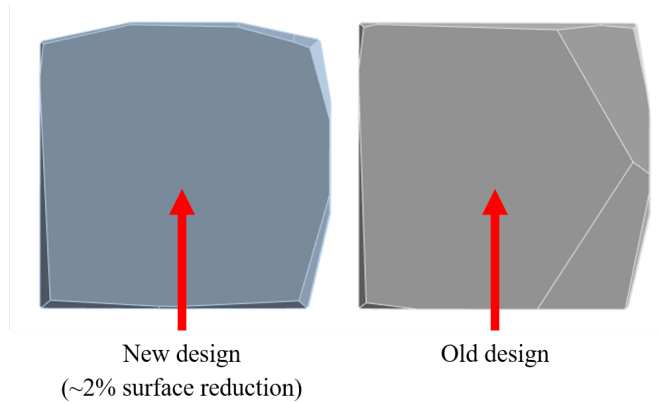


New design
(~2% surface reduction)

Old design

Figure 5.1: *3D model of the TZM tiles for integral calculation*

The idea of this analysis is to apply a heat flux on the plasma facing surface and a set temperature $(20°C)$ at the back of the tile. This allows to calculate the power needed to assure $(20°C)$ at the backside of the tile. According to the theory of conductivity, the heat

flow entering the tile should be the same as the heat flow evacuated at the back. This can be calculated analytically using the integral form of Fourier's law. (*see* 2.3.2)

$$\oiint_S \mathbf{q} \cdot d\mathbf{S} = -k \oiint_S \nabla T \cdot d\mathbf{S} \qquad [W] \quad (5.1)$$

The left hand side of the equation 5.1 is the thermal power $\partial_t Q$ in $[W]$ transferred by conduction and defined as $\partial_t Q := \oiint_S \mathbf{q} \cdot d\mathbf{S}$. The differential $d\mathbf{S}$ is an oriented surface area element in $[m^2]$. On the right hand side of the equation is surface integral of the dot product between the temperature gradient $\nabla T$ and an oriented surface area element $d\mathbf{S}$. To integrate this equation, it is assumed that the material is homogeneous with constant thermal conductivity. It is then possible to integrate 5.1 for a 1-D geometry between two points. The result of the integration gives the following expression for heat flow expression:

$$\partial_t Q = -k \frac{A}{L} \Delta T \qquad [W] \quad (5.2)$$

In this expression, $A$ is the cross-sectionnal area perpendicular to the heat flux in $[W]$, $L$ is the distance between the two surfaces in $[m]$, $\Delta T$ is the temperature difference between both front and back surfaces and $k$ is the thermal conductivity of the medium in $[W/m^2 K]$. The cross-sectionnal area $A$ and the length $L$ are assumed constant as well as the thermal conductivity $k$. It is possible to determine the heat flow flowing through the tile and the heat flow evacuated through the boundary condition, they should be equal to satisfy energy conservation. Based on this, it is possible to use a model to approximate the heat flow through the tile.
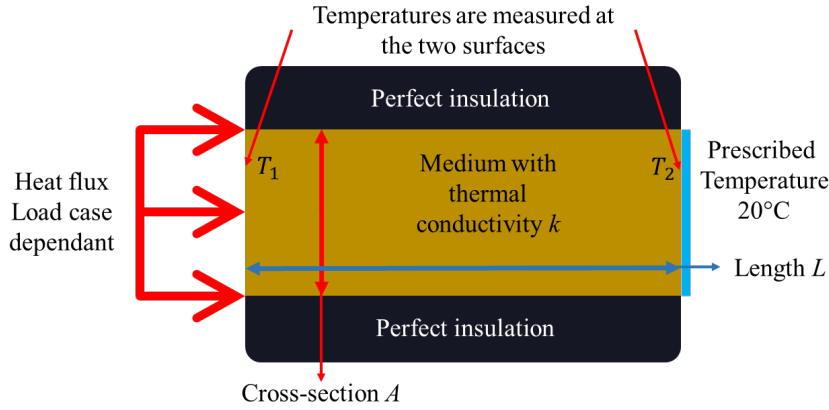


Figure 5.2: *Model of the 1-D conduction test*

According to 5.2, the evolution of the temperature inside the medium is linear. It is then possible to calculate the heat flow flowing in and out (resp. $\partial_t Q_{in}$ and $\partial_t Q_{out}$). The idea is to find what heat flow $\partial_t Q_{out}$ is needed in order to respect the prescribed temperature boundary condition. After some calculations, it was found that $\partial_t Q_{in} = -\partial_t Q_{out}$. This validates the idea of calculating the surface integral using ANSYS®. The solver settings of the ANSYS® project are by default progam controlled. Since the calculation isn't too complex, it is acceptable to continue with these settings. Prescribed temperatures at the back of the TZM tiles were defined and set to $20°C$ (it is also important to keep in mind that the backside

temperature doesn't affect the value of the integrales, any arbitrary temperature will work).
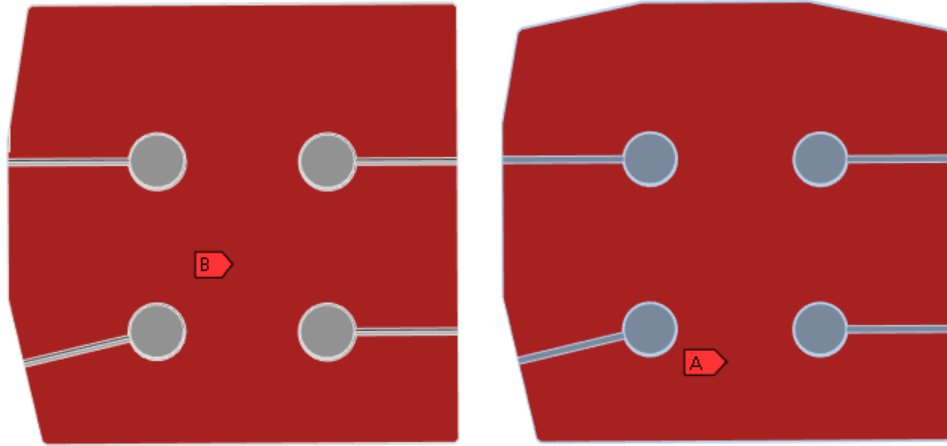


Figure 5.3: *Prescribed temperature of the ANSYS® model for surface integral calculations*

The loadcases are the standard loadcases chosen to analyse the tile assembly. They are

|  | *w = 8* | | | *w = 16* | | |
|---|---|---|---|---|---|---|
|  | *t = 0* | *t = 1* | *t = 2* | *t = 0* | *t = 1* | *t = 2* |
| *dir = 1* | | | | | | |
| *c* | 0.0790 | 0.1692 | 0.2945 | 0.3670 | 0.7187 | 3.1815 |
| *c* | -0.8651 | 50.0476 | 5.9384 | -9.0714 | 297.0923 | 46.2143 |
| *c* | 124.2756 | -50.9612 | -14.2721 | 128.2265 | -630.5455 | -381.0930 |
| *dir = 0* | | | | | | |
| *c* | 0.0357 | 1.2473 | 0.2119 | 0.3593 | -0.2755 | 2.1764 |
| *c* | -17.9048 | -37.1111 | 8.8591 | -30.7381 | -9.5952 | -3.0000 |
| *c* | 105.5518 | 232.1160 | -94.7351 | 100.2497 | 141.2778 | -259.7326 |

Table 5.1: Caption

### 5.1.2　Comparison between old and new TZM tile design

### 5.1.3　Film coefficient influence on thermal behavior

### 5.1.4　Loadcase influence on thermal behavior

## 5.2　TRANSIENT THERMAL ANALYSIS

## 5.3　STATIC STRUCTURAL ANALYSIS

## 5.4　COUPLED FIELDS ANALYSIS

# 6 | CONCLUSION AND RECOMMENDATIONS

intro to ch6

# Bibliography

[1] Y. Cengel. *Heat Transfer: A Practical Approach*. McGraw-Hill Education, 2004. ISBN: 9780071236447. URL: https://books.google.de/books?id=xYASMQAACAAJ.

[2] Bernd Diekmann and Eberhard Rosenthal. *Energie: Physikalische Grundlagen ihrer Erzeugung, Umwandlung und Nutzung*. de. Wiesbaden: Springer Fachmedien Wiesbaden, 2014. ISBN: 9783658005009 9783658005016. DOI: 10.1007/978-3-658-00501-6. URL: https://link.springer.com/10.1007/978-3-658-00501-6 (visited on 05/08/2024).

[3] J. Fellinger. *Thermal-mechanical assessment of heat shields and baffles*. Tech. rep. 28Y3JJ. Wendelsteinstraße 1, Greiswald, Germany: Max-Planck Institute for Plasma Physics, May 2013.

[4] Jeffrey P. Freidberg. *Plasma Physics and Fusion Energy*. Cambridge University Press, 2007.

[5] J. H. Lienhard V and J. H. Lienhard IV. *A Heat Transfer Textbook*. Version 6.00. Cambridge, MA, Apr. 2024. URL: https://ahtt.mit.edu.

[6] UDVARDY MIKLOS D. F. "THE ROLE OF THE FEET IN BEHAVIORAL THERMOREGULATION OF HUMMINGBIRDS". en. In: *The Cooper Ornithological Society* (1983). URL: https://sora.unm.edu/sites/default/files/journals/condor/v085n03/p0281-p0285.pdf.

[7] Jiawu Zhu. *Parametric thermal and mechanical analysis of ECRH reflecting tile (TZM)*. 2019.